UC Irvine

UC Irvine Previously Published Works

Title

Femtosecond X-ray Spectroscopy Directly Quantifies Transient Excited-State Mixed Valency

Authors

Liekhus-Schmaltz, Chelsea

Fox, Zachary W

Andersen, Amity

et al.

Peer reviewed

Femtosecond X-ray Spectroscopy Directly Quantifies Transient Excited State Mixed Valency

Chelsea Liekhus-Schmaltz,[*,1] *Zachary W. Fox,*[1] *Amity Andersen,*[2] *Kasper S. Kjaer,*[3,4] *Roberto Alonso-Mori,*[5] *Elisa Biasin,*[3,||] *Julia Carlstad,*[1,⊥] *Matthieu Chollet,*[5] *James D. Gaynor,*[1,⊥] *James M. Glownia,*[5] *Kiryong Hong,*[6,#] *Thomas Kroll,*[7] *Jae Hyuk Lee,*[6,∇] *Benjamin I. Poulter,*[1] *Marco Reinhard,*[3] *Dimosthenis Sokaras,*[7] *Yu Zhang,*[8,‡‡] *Gilles Doumy,*[9] *Anne Marie March,*[9] *Stephen H. Southworth,*[9] *Shaul Mukamel,*[8] *Amy Cordones-Hahn,*[3] *Robert W. Schoenlein,*[3,5] *Niranjan Govind,*[*,§§] *and Munira Khalil*[*,1]

[1]Department of Chemistry, University of Washington, Seattle, WA, USA.

[2]Environmental Molecular Sciences Laboratory, Earth and Biological Sciences Directorate, Pacific Northwest National Laboratory, Richland, WA, USA.

[3]Stanford PULSE Institute, SLAC National Accelerator Laboratory, Menlo Park, CA, USA.

[4]Department of Physics, Technical University of Denmark, Kongens Lyngby, Denmark.

[5]Linac Coherent Light Source, SLAC National Accelerator Laboratory, Menlo Park, CA, USA.

[6]Ultrafast X-ray Science Laboratory, Chemical Sciences Division, Lawrence Berkeley National Laboratory, Berkeley, CA, USA

[7]SSRL, SLAC National Accelerator Laboratory, Menlo Park, CA, USA

[8]Department of Chemistry, and Physics & Astronomy, University of California, Irvine, CA, USA

[9]Chemical Sciences and Engineering Division, Argonne National Laboratory, Lemont, IL, USA

[10]Physical Sciences Division, Physical and Computational Sciences Directorate, Pacific Northwest National Laboratory, Richland, WA, USA

Corresponding Authors

* cliekhus@uw.edu; niri.govind@pnnl.gov; mkhalil@uw.edu

Quantifying charge delocalization associated with short-lived photoexcited states of molecular complexes in solution remains experimentally challenging, requiring local element specific femtosecond experimental probes of time-evolving electron transfer. In this study, we quantify the evolving hole charge distribution in the photoexcited charge transfer state of a prototypical mixed valence bimetallic iron-ruthenium complex, $[(CN)_5Fe^{II}CNRu^{III}(NH_3)_5]^-$, in water by combining femtosecond X-ray spectroscopy measurements with time-dependent density functional theory calculations of the excited-state dynamics. We estimate the hole charge accumulated at the Fe atom to be 0.6 ± 0.2, resulting from excited-state metal-to-metal charge transfer, on a ~60 fs timescale. Our combined experimental and computational approach provides a spectroscopic ruler to quantify excited state valency in solvated complexes.

The field of inorganic mixed valency has contributed significantly to our fundamental understanding of intramolecular electron transfer since the synthesis of the Creutz-Tuabe ion reported in 1969.[1] One of the questions in the field of mixed valency that continues to garner much experimental and theoretical interest is the precise determination of the extent of electron delocalization.[2-3] Electron delocalization has largely been studied under the Robin-Day classification system, which attributes the extent of delocalization to electronic coupling between two metal centers: Class I (uncoupled, localized charges), Class II (moderately coupled), Class III (strongly coupled, delocalized charges).[4] The Robin-Day classification is based on IR and near IR spectroscopy, which are indirect probes of the valence charge distribution, making quantitative determinations of electron delocalization between the transition metal centers a challenging problem. The challenge is compounded when trying to determine mixed valency associated with short-lived excited electronic states. The lack of direct experimental measurements of ultrafast time-evolving electronic character makes quantitative connection to theory difficult, resulting in a significant knowledge gap for developing predictive design principles to harness molecular mixed valency for molecular energy capture or electron transfer in chromophore-catalyst assemblies.

Time-resolved optical, infrared (IR), and 2D spectroscopies have made important measurements of ultrafast charge transfer in transition metal mixed valence systems by measuring relevant solvent-dependent kinetic parameters of electron transfer and identifying the role of the coupled high-frequency cyanide vibrations in the photoinduced forward and back electron transfer processes.[5-13] However, ultrafast optical and IR studies are inherently limited in their ability to map electronic dynamics at high spatial resolution making it challenging to determine the extent of ultrafast excited state mixed valency in molecular systems. In contrast to ultrafast optical and IR studies, time-resolved X-ray absorption and X-ray emission spectroscopies (XAS and XES) probe

transitions involving core level atomic orbitals, making them selective and sensitive to local atomic and electronic changes.[14-20] Recent advances in X-ray Free Electron Lasers (XFELs), such as the Linac Coherent Light Source (LCLS), enable the production of high-intensity, tunable, < 45 fs X-ray pulses for ultrafast XES and XAS measurements of atomic and electronic structural dynamics of dilute solution samples.[21-22] These time resolved X-ray studies have successfully monitored excited state dynamics such as spin crossovers, nuclear oscillations, and electron transfer in solvated transition metal complexes.[23-33]

Obtaining quantitative microscopic information from ultrafast X-ray experiments requires accompanying simulations of the transient signals on electronic excited states. In the case of the mixed valence complexes, it is crucial to include explicit solute-solvent interactions to correctly model the electronic excited state dynamics.[34] Currently the state-of-the-art theoretical techniques to tackle transition metal complexes are based on wavefunction approaches.[35] However, these methods become computationally prohibitive for large solvated systems lacking high symmetry. In previous work, we have shown that ground-state quantum mechanics/molecular mechanics (QM/MM) dynamics at the density functional theory (DFT) level and excited-state computations with linear-response time-dependent density functional theory (LR-TDDFT) are sufficiently accurate to capture the ground-state and excited-state characteristics of these large, solvated transition metal complexes.[34, 36-37] This has allowed us to analyze how the local solvation environment and explicit solute-solvent interactions influence the intensity and line shape of specific spectroscopic features from the infrared to X-ray wavelengths.[36]

In this Letter, we present a combined experimental and computational study to quantify the extent of ultrafast electron delocalization on the short-lived metal-to-metal charge transfer (MMCT) state of the mixed valence complex, $[(CN)_5Fe^{II}CNRu^{III}(NH_3)_5]^-$, FeRu for brevity, using

femtosecond XAS at the Fe K-edge.[3,32–34] We use a high resolution XAS technique, high energy-resolution fluorescence X-ray absorption near edge spectroscopy (HERFD-XANES). This method can be used to monitor small spectral changes in absorption by detecting fluorescence X-ray photons emitted through a longer lived intermediate state (with respect to the core-hole state) resulting in an almost background-free measurement with reduced spectral broadening that yields a high resolution absorption spectrum.[38-44] FeRu has a MMCT transition in the near IR region of the UV-Vis spectrum (λ_{MMCT} = 961 nm). Excitation into this broad band initiates an intramolecular charge transfer from the Fe to the Ru atom. Transient optical experiments have reported an ultrafast back electron transfer (BET) time of 89 ± 10 fs, and time-resolved Kβ emission reported a BET of 62 ± 10 fs.[9, 34] Two-dimensional vibrational-electronic spectroscopy has shown that the MMCT is strongly coupled to the cyanide bridge stretching mode in FeRu,[12] and a recent ultrafast X-ray scattering experiment of aqueous FeRu discovered that coherent motions of the first solvation shell play an important role in the ultrafast BET dynamics.[34] While these experiments measure vibronic coupling and solute-solvent interactions, they are limited in their ability to measure the time-resolved, non-equilibrium electron delocalization, which is a key property governing electron transfer dynamics.[2-3, 45-46] In this study, we use ultrafast HERFD-XANES measurements and perform a computational study of the excited state transient XANES spectroscopy based on LR-TDDFT to study electron delocalization between the two metal centers in FeRu by directly probing the valency of the Fe atom immediately following a MMCT excitation.

To measure the time-resolved valency of FeRu in aqueous solution, we performed an optical pump, HERFD-XANES probe experiment at the X-ray Pump Probe (XPP) endstation at LCLS as shown in Fig. 1a.[47] The MMCT transition in FeRu is excited at 800 nm and the HERFD-XANES measurement is performed by recording the X-ray emission intensity at the peak of the
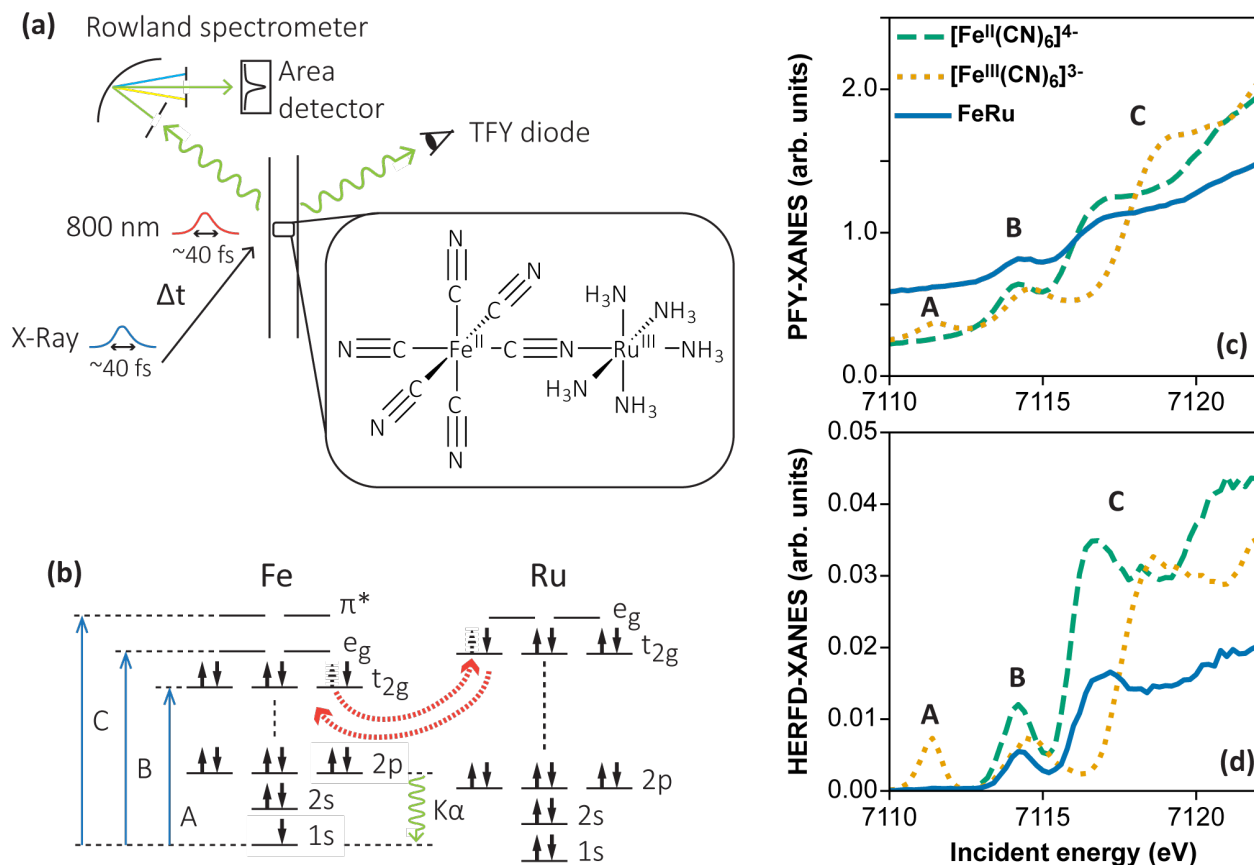
Figure 1. (a) Experimental configuration at the XPP endstation at LCLS to perform transient HERFD-XANES. The sample, 30 mM of FeRu (shown in the inset) dissolved in water is delivered via a 50 μm circular liquid jet in a He filled chamber. The MMCT transition is excited using a ~40 fs FWHM, 800 nm, pulse and probed with a ~40 fs FWHM long X-ray pulse whose incident energy is scanned from 7110 – 7120 eV using an upstream monochromator (not shown). (b) The relevant atomic and molecular orbitals in FeRu. The MMCT excitation and resulting BET are shown as the red dashed line and the core-level transitions probed by the X-ray probe are shown as blue arrows. The HERFD-XANES probe is scanned over the 1s to t_{2g}, e_g, and $\pi*$ transitions, and the peaks are labeled as A, B, and C respectively. The time-resolved HERFD-XANES fluorescence signal is measured at the peak of the Kα1 (2p$_{3/2}$→1s) transition by the Rowland spectrometer, shown by the green line. The ground state XANES (in partial fluorescence yield (PFY) mode) and HERFD-XANES spectra of FeRu (30 mM) and two model complexes, K$_4$Fe^{II}(CN)$_6$ (100 mM) and K$_3$Fe^{III}(CN)$_6$ (100 mM), in aqueous solutions, at the Fe K-edge are shown in (c) and (d) respectively. For all three complexes, the B (1s→3de_g) and C (1s→ $\pi*$) peaks are visible, while the A (1s→3dt_{2g}) peak only appears in the spectra of K$_3$Fe^{III}(CN)$_6$ because of a t_{2g} vacancy. Comparing the XANES measurement taken in the PFY mode and the HERFD-XANES spectra shows how HERFD-XANES spectroscopy method significantly reduces the background. The PFY-XANES spectra are obtained by summing over the emission frequencies of the Resonant Inelastic X-ray Scattering (RIXS) spectral maps. See Fig S5 in the Supporting Information for further details.

details are provided in the Experimental Section and Sections 2 and 3 of the Supporting Information. To understand how signatures of oxidation state and metal-ligand interactions are encoded in the HERFD-XANES spectra, we plot the ground state XANES (Fig. 1c) and HERFD-XANES (Fig. 1 d) spectra of FeRu as well as two model complexes, $K_4Fe^{II}(CN)_6$ and $K_3Fe^{III}(CN)_6$ in aqueous solution measured at a synchrotron. A comparison of the XANES and HERFD-XANES reveals a large decrease in background and a decrease in peak-widths of the spectral features in the latter measurement. The XANES-HERFD measurement better isolates the fluorescence line of interest from the background allowing for the detection of small changes in the XANES spectral features.

While the HERFD-XANES spectrum is dependent on the cross-sections for both absorption and $K\alpha_1$ emission, the primary factor determining the energy-dependence of the HERFD-XANES intensity is the variation of the absorption cross-section for each incident energy. Therefore, we can associate each peak with an absorption transition.[44] The characteristics of the X-ray near edge spectra for Fe(II) and Fe(III) model complexes dissolved in water have been discussed extensively in the literature,[36, 48] and are summarized in Figure 1 as peaks A, B, and C. Briefly, both Fe(II) and Fe(III) cyanide complexes exhibit peaks B and C that correspond to excitations of electrons from the 1s Fe core orbital to the metal e_g and ligand π^* molecular orbitals, respectively. The A peak is present only in the Fe(III) complex and indicates the presence of a hole in the t_{2g} molecular orbital. Peak A serves as an important spectral marker for monitoring the oxidation state of the Fe atom. We also observe a blue shift of the B and C features by ~0.5 and ~2 eV, respectively, upon oxidation of the Fe(II) complex. The ground state HERFD-XANES spectrum of FeRu shows peaks B and C, characteristic of an Fe(II) complex, at 7114 eV and 7117 eV, respectively. Figure S4 in the Supporting Information compares the experimental and

calculated XANES spectra of FeRu in its electronic ground state. The ground state XANES calculations, performed at the LR-TDDFT level, account for explicit solute-solvent interactions, which are necessary to capture the features of the experimental spectrum.

In Fig. 2 (b) we present the transient HERFD-XANES measurement of FeRu to characterize the short-lived mixed valence excited state formed upon MMCT excitation. The
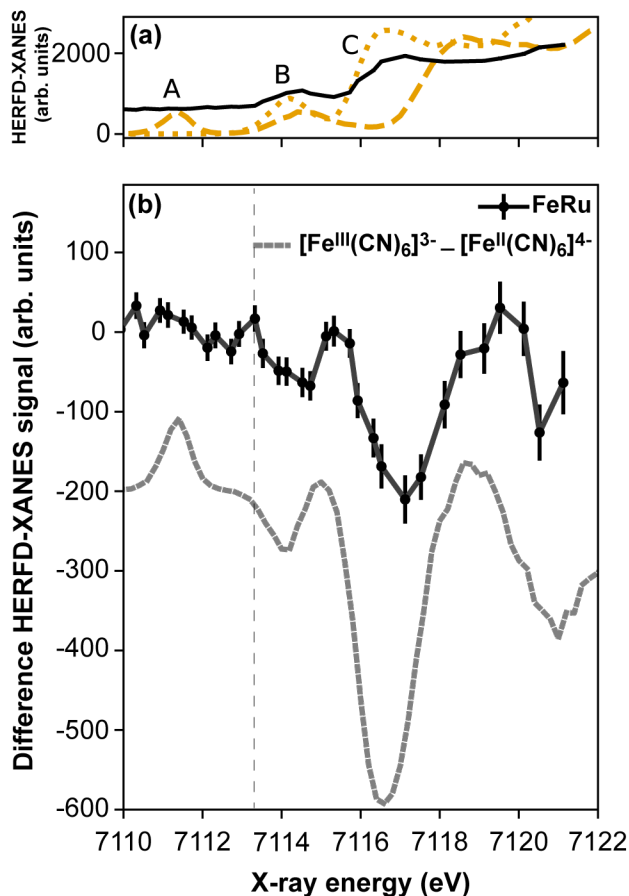

Figure 2. Transient HERFD-XANES signal. (a) The ground state HERFD-XANES spectra of FeRu taken at LCLS (black solid), $[Fe^{II}(CN)_6]^{4-}$ (yellow dotted) taken at APS, and $[Fe^{III}(CN)_6]^{3-}$ (yellow dashed) taken at APS. Since the excited state FeRu HERFD-XANES spectra is measured at the peak of the ground state $K\alpha_1$ line, we also show the $[Fe^{III}(CN)_6]^{3-}$ HERFD-XANES spectra at the peak of the $[Fe^{II}(CN)_6]^{4-}$ $K\alpha_1$ line. (b) The difference spectra between the excited and ground state FeRu spectra is shown as black circles in the lower panels. To compare, the difference between the two model complexes is shown vertically offset in the grey dashed line. The difference of the model complex spectra is scaled by the excitation fraction of 0.25 and the difference in concentration of the model complexes and FeRu.

9

transient signal is plotted as the difference between the excited and the ground state HERFD-XANES spectra summed over the optical pump/X-ray jitter delays between -35 fs and 35 fs. This delay range was chosen to cover the initial MMCT excitation and accounting for the ~62 fs lifetime of the excited state.[34] The data shows that the B and C features shift to the blue to ~7115 eV and ~7119 eV, respectively. In addition, a new peak appears in the difference spectrum at ~7113 eV. To relate the observed changes in the transient HERFD-XANES spectrum to the mixed valency in the excited state of FeRu, we compare it to the difference between the ground state HERFD-XANES spectra (Fig. 2(a)) of the Fe(III) from the Fe(II) model complexes (grey dashed in Fig. 2(b)). The model complex difference has been scaled to account for an excitation factor of 25% in the experiment as determined from a concurrent Kβ XES measurement.[34] The similarity in the dispersive lineshapes for peaks B and C in the FeRu transient spectrum and the difference spectrum of the model complexes confirms that the MMCT from the Fe to the Ru results in an increase in the oxidation state of the Fe atom. Interestingly, the new feature at ~7113 eV in the FeRu spectrum is significantly blue shifted compared to the A feature of the Fe(III) complex at ~7111 eV suggesting that the transient Fe atom oxidation state is a fractional value between +2 and +3.

Developing a quantitative understanding of the experimental fs XANES-HERFD data in Figure 2b required computations of the transient Fe K-edge XANES at several points along the MMCT excited state (see Section 4 in the Supporting Information for details). Briefly, excited state geometries were computed by optimizing clusters of the solvated FeRu complex (extracted from an equilibrated ground state QM/MM calculation) on the MMCT surface. Transient Fe K-edge XANES computations were performed on these excited-state geometries by first converging the appropriate reference MMCT valence state in combination with the maximum overlap method implemented in NWChem.[49-50] The MMCT excited state optimizations were performed with LR-

TDDFT gradients,[18] while the XANES calculations were performed with the restricted excitation window LR-TDDFT approach,[19] including higher-order contributions to the oscillator strengths to capture the quadrupolar nature of the pre-edge transitions at the Fe K-edge. The computed XANES
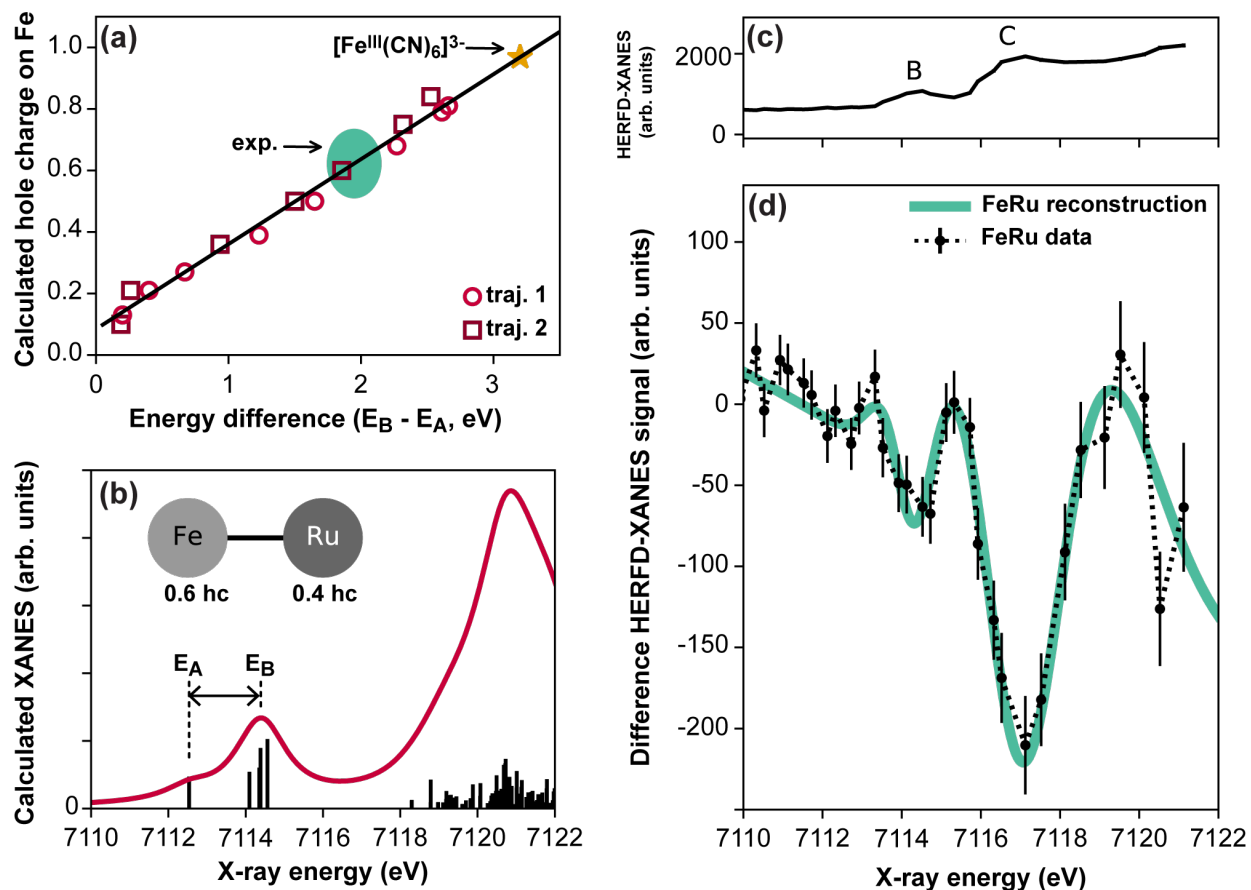

Figure 3. **Computed and measured hole charge on the excited state of FeRu.** (a) The computed Fe hole charge as a function of the A-B peak splitting in calculated transient Fe K-edge XANES spectra for two separate MMCT excited-state optimization trajectories (traj. 1 and 2). For comparison, the splitting between the A and B peak for the ground state experimental and computed $[Fe^{III}(CN)_6]^{3-}$ XANES spectrum is given by the yellow star (Ref. 36). (b) The computed excited state XANES spectrum for calculated Fe hole of 0.6. The arrows indicate the positions of the calculated A and B peaks used to construct the linear relationship in Fig. 3a. (c) The ground state HERFD-XANES spectra of FeRu taken at LCLS. (d) The experimental difference spectrum between the excited and ground state FeRu XANES-HERFD spectra is shown as black circles in the lower panels. To measure the A and B peak positions, we reconstruct the difference spectrum using the ground state FeRu spectrum, resulting in a measured A-B peak splitting of 1.9 ± 0.4 eV. The corresponding experimental measurement of the hole charge on FeRu using the spectral ruler in Figure 3a is shown as the green oval with the uncertainty given by its size.

spectra at various points along the MMCT excited state from a representative optimization trajectory are plotted in Figure S10 of the Supporting Information. These points correspond to different excited state hole charges on the Fe atom (given by the Mulliken and Löwdin populations). The calculated excited state XANES spectra for different hole charges on the Fe atom reveal differences in the energy separation of the peaks A and B. For each hole charge, the computed A peak energy is given by the lowest energy transition, and the computed B peak energy is given by the broadened B peak transitions (E_B-E_A, Fig. 3b). As shown in Fig. 3 a, we find a nearly linear relation between the energy difference of the and B peaks with the Fe hole charge. Additionally, we note that the experimentally measured and calculated peak separation of model complex, $[Fe^{III}(CN)_6]^{3-}$,[36] shown with a yellow star, also lies on the calculated linear line in Figure 3a. The physical interpretation of the calculated linear relationship between the Fe hole charge and the peak separation in the XANES spectra can be explained by noting that the crystal field splitting is approximately proportional to the magnitude of the dipole on the MMCT. Furthermore, the energy separation is proportional to the charge difference between the two metal centers as the system evolves on the MMCT state, given that the very short lifetime of the MMCT state (~62 fs) precludes any significant structural rearrangement.[34] This allows us to use this linear relation as a spectral ruler for determining the Fe hole charge.

We use the computed linear relationship between the hole charge on the Fe atom and the A-B splitting to estimate the experimental hole charge on the Fe atom after the MMCT excitation. To extract the experimentally measured A-B splitting, we fit the difference spectrum using a function constructed from the difference of Gaussians at each A, B, and C peak for the excited state spectrum and another sum of Gaussians for the ground state spectrum, scaled to the excitation fraction of 0.25 determined by Reference 34. To reduce the number of fit parameters, we use the

peak positions, amplitudes, and widths of the ground state B and C peaks determined by fitting two gaussians and an error function to approximate the absorption edge to the FeRu ground state XANES-HERFD spectrum. We also include a linear background to approximate the difference between the excited state and ground state absorption edges. At energies near the A and B peaks, this approximation is valid because the peak amplitudes are greater than or similar to the magnitude of the absorption edge. However, at higher photon energies the absorption edge is larger in amplitude than the C peak, invalidating the approximation. For this reason, the linear background approximation breaks down and the position and amplitude of the excited C peak is likely inaccurate. It would be possible to add higher order terms to the background function. However, since we are only interested in fitting the A and B peaks, doing so unnecessarily adds additional terms to the fit which could lead to an overfitting of the data. This is a particular risk in this case given the low resolution of signal. We also note a feature near 7111 eV of similarly sized amplitude to the fitted A peak. An A peak in this region would result in a greater than 3 eV splitting between the A and B peak, which corresponds to a hole charge greater than 1. This is unphysical, and we therefore eliminate this possibility. Section 3.5 of the Supporting Information details the fit values and the final reconstruction is shown as the thick green line in Fig. 3. The final excited state A and B peak positions are 7113.8 eV and 7115.7 eV.

Applying the linear relationship found between the calculated hole charges and A-B peak splitting, we estimate that the hole charge on the Fe atom over the time duration of our transient measurement is $\approx 0.6 \pm 0.2$. This hole charge value indicates that the charge is relatively delocalized across the Fe and Ru atoms. This is pictorially depicted by plotting the transition densities associated with peak A in the calculated excited state XANES spectra for two different excited state configurations of FeRu on the MMCT surface. When the hole is primarily on the Ru
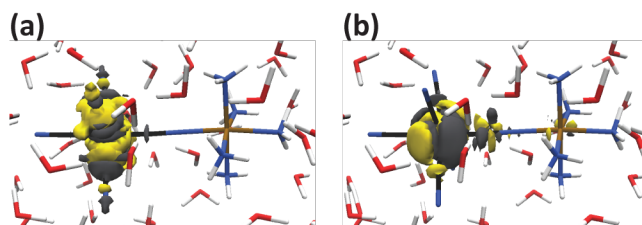
Figure 4: Calculated A transition density plots. The negative density is grey while the positive density is yellow. (a) A peak transition for a 0.1 Fe hole charge. (b) A peak transition for a 0.60 Fe hole charge.

atom, we see electron density localized on the Fe atom in FeRu (Fig. 4 a). In contrast, the electron density is shared between the bridging cyanide ligand and the Ru atom when the hole charge is 0.6 on the Fe atom (Fig. 4 b) providing a view of the local electronic structure of the experimentally measured MMCT excited state of FeRu with a lifetime of ~65 fs.

The experimentally determined value of 0.6 hole charge on Fe using the spectroscopic ruler (Fig. 3a), indicates that the short-lived MMCT excited state is more delocalized than the ground state in FeRu. Previous transient optical and IR experiments have determined timescales of the back electron transfer and the subsequent excitation of the high frequency cyanide stretching modes in the non-equilibrium ground state. However, those experiments have been unable to measure the electronic character of the short lived MMCT state in FeRu. This experiment and the plotted transition densities in Fig 4 showing electron delocalization across the cyanide bridging ligand connect with previously measured 2D VE spectra of FeRu in formamide where the vibronic coupling between the MMCT excitation and the cyanide stretching frequencies, was strongest for the bridging mode.[12-13]

Our measurement of the Fe hole charge demonstrates how time-resolved HERFD-XANES spectroscopy combined with novel excited-state calculations can provide detailed information about the electron density in excited state mixed-valence metal complexes. With further XFEL

enhancements, we expect that the time-resolved HERFD-XANES demonstrated here will become an important tool for studying electron delocalization in nonequilibrium conditions. In particular, the ability to measure time-evolving HERFD-XANES spectra in the first 100 fs following optical excitation will provide key insights into electron transfer mechanisms and accompanying dynamics in complex molecular systems in realistic environments

Experimental Methods

As shown in part (a) of Fig. 1, 30 mM of aqueous FeRu is introduced into the experiment via a 50 μm round jet. A 4 μJ, 40 fs full width half max (FWHM), 800 nm laser pulse with a 100 by 120 μm focus excites FeRu to the MMCT state. This pulse intensity is within the linear excitation regime, as determined by Kβ emission in Reference 34, which was measured in concert with this experiment. The excited state is probed with time overlapped 45 fs FWHM X-ray pulses at 120 Hz. The incident X-ray energy is scanned below the Fe K-edge using a 1 eV bandwidth Si(111) channel-cut monochromator, reducing the X-ray flux to 10^{10} photons per pulse with a 20-25 μm focus. For each pump probe event, the time-delay between the laser and X-ray pulses is measured using the XPP timing tool.[47, 51]

The HERFD-XANES measurement is performed by recording the X-ray emission intensity at the peak of the ground state Kα_1 emission line using a Rowland monochromatic analyser crystal and image area detector with 0.4 eV resolution while scanning the incoming X-ray photon energy. The alignment of the spectrometer to the Kα_1 line is verified in Fig. S6 of the Supporting Information. The spectrometer intensity is then normalized to the pulse intensity according to Eq. 1 of the Supporting Information. Similar measurements of FeRu and two model complexes,

$K_4Fe^{II}(CN)_6$ and $K_3Fe^{III}(CN)_6$, were taken at beamline 7-ID-D at the Advanced Photon Source (APS) at Argonne National Laboratory using the same conditions described previously.[36]

Computational Methods

All ground and excited state calculations for this study were performed with the NWChem computational chemistry program.[49-50] We performed 1) ground state quantum mechanics/molecular mechanics (QM/MM) calculations (minimization and molecular dynamics), 2) LR-TDDFT based excited state calculations were performed on sufficiently large solvated clusters ($\approx$ 238 atoms), including the FeRu complex and explicit waters that were extracted from the QM/MM simulations, 3) LR-TDDFT based excited state optimizations on the MMCT excited state on the clusters, and 4) transient Fe K-edge XANES calculations using the restricted energy window LR-TDDFT approach on structures along the MMCT excited state surface. Details of all the calculations including the calculation settings are given in Section 4 of the Supporting Information.

ASSOCIATED CONTENT

Supporting Information. The following files are available free of charge.

Materials and ground state IR, UV-Vis, XANES and HERFD-XANES spectroscopy, details of data analysis of femtosecond HERFD-XANES and a complete description of the computational work. (PDF)

AUTHOR INFORMATION

Notes

||Present Address: Environmental Molecular Sciences Laboratory, Earth and Biological Sciences Directorate, Pacific Northwest National Laboratory, Richland, WA, USA

⊥Present Address: Department of Chemistry, University of California, Berkeley, CA, USA.

#Present Address: Gas Metrology Group, Division of Chemical and Biological Metrology, Korea Research Institute of Standards and Science, Daejeon, Republic of Korea.

∇Present Address: Pohang Accelerator Laboratory, Pohang, Republic of Korea.

‡‡Present Address: Q-Chem, Pleasanton, CA, USA.

ACKNOWLEDGMENT

REFERENCES

1.   Creutz, C.; Taube, H. Direct approach to measuring the Franck-Condon barrier to electron transfer between metal ions. *Journal of the American Chemical Society* **1969,** *91* (14), 3988-3989 DOI: 10.1021/ja01042a072.

2.   Kubiak, C. P. Inorganic Electron Transfer: Sharpening a Fuzzy Border in Mixed Valency and Extending Mixed Valency across Supramolecular Systems. *Inorganic Chemistry* **2013,** *52* (10), 5663-5676 DOI: 10.1021/ic302331s.

3.   Demadis, K. D.; Hartshorn, C. M.; Meyer, T. J. The Localized-to-Delocalized Transition in Mixed-Valence Chemistry. *Chemical Reviews* **2001,** *101* (9), 2655-2686 DOI: 10.1021/cr990413m.

4.   Robin, M. B.; Day, P. Mixed Valence Chemistry-A Survey and Classification. In *Advances in Inorganic Chemistry and Radiochemistry*, Emeléus, H. J.; Sharpe, A. G., Eds. Academic Press: 1968; Vol. 10, pp 247-422.

5.   Wang, C.; Mohney, B. K.; Akhremitchev, B. B.; Walker, G. C. Ultrafast Infrared Spectroscopy of Vibrational States Prepared by Photoinduced Electron Transfer in

(CN)5FeCNRu(NH3)5-. *The Journal of Physical Chemistry A* **2000,** *104* (18), 4314-4320 DOI: 10.1021/jp993927y.

6.   Tominaga, K.; Kliner, D. A. V.; Johnson, A. E.; Levinger, N. E.; Barbara, P. F. Femtosecond experiments and absolute rate calculations on intervalence electron transfer of mixed-valence compounds. *The Journal of Chemical Physics* **1993,** *98* (2), 1228-1243 DOI: 10.1063/1.464344.

7.   Tivanski, A. V.; Wang, C.; Walker, G. C. Vibrational Mode Coupling to Ultrafast Electron Transfer in [(CN) $_5$ OsCNRu(NH $_3$) $_5$] $^-$ Studied by Femtosecond Infrared Spectroscopy. *The Journal of Physical Chemistry A* **2003,** *107* (43), 9051-9058 DOI: 10.1021/jp034274v.

8.   Slenkamp, K. M.; Lynch, M. S.; Van Kuiken, B. E.; Brookes, J. F.; Bannan, C. C.; Daifuku, S. L.; Khalil, M. Investigating vibrational anharmonic couplings in cyanide-bridged transition metal mixed valence complexes using two-dimensional infrared spectroscopy. *The Journal of Chemical Physics* **2014,** *140* (8), 084505 DOI: 10.1063/1.4866294.

9.   Reid, P. J.; Silva, C.; Barbara, P. F.; Karki, L.; Hupp, J. T. Electronic Coherence, Vibrational Coherence, and Solvent Degrees of Freedom in the Femtosecond Spectroscopy of Mixed-Valence Metal Dimers in H2O and D2O. *The Journal of Physical Chemistry* **1995,** *99* (9), 2609-2616 DOI: 10.1021/j100009a019.

10.   Lynch, M. S.; Van Kuiken, B. E.; Daifuku, S. L.; Khalil, M. On the Role of High-Frequency Intramolecular Vibrations in Ultrafast Back-Electron Transfer Reactions. *The Journal of Physical Chemistry Letters* **2011,** *2* (17), 2252-2257 DOI: 10.1021/jz200930h.

11.   Lynch, M. S.; Slenkamp, K. M.; Khalil, M. Communication: Probing non-equilibrium vibrational relaxation pathways of highly excited C≡N stretching modes following ultrafast back-

electron transfer. *The Journal of Chemical Physics* **2012,** *136* (24), 241101   DOI: 10.1063/1.4731882.

12.   Fox, Z. W.; Blair, T. J.; Khalil, M. Determining the Orientation and Vibronic Couplings between Electronic and Vibrational Coordinates with Polarization-Selective Two-Dimensional Vibrational-Electronic Spectroscopy. *The Journal of Physical Chemistry Letters* **2020,** *11* (4), 1558-1563 DOI: 10.1021/acs.jpclett.9b03752.

13.   Courtney, T. L.; Fox, Z. W.; Estergreen, L.; Khalil, M. Measuring Coherently Coupled Intramolecular Vibrational and Charge-Transfer Dynamics with Two-Dimensional Vibrational–Electronic Spectroscopy. *The Journal of Physical Chemistry Letters* **2015,** *6* (7), 1286-1292 DOI: 10.1021/acs.jpclett.5b00356.

14.   Bressler, C.; Chergui, M. Ultrafast X-ray Absorption Spectroscopy. *Chemical Reviews* **2004,** *104* (4), 1781-1812 DOI: 10.1021/cr0206667.

15.   Gaffney, K. J. Capturing photochemical and photophysical transformations in iron complexes with ultrafast X-ray spectroscopy and scattering. *Chem Sci* **2021,** *12* (23), 8010-8025 DOI: 10.1039/d1sc01864g.

16.   Bergmann, U.; Kern, J.; Schoenlein, R. W.; Wernet, P.; Yachandra, V. K.; Yano, J. Using X-ray free-electron lasers for spectroscopy of molecular catalysts and metalloenzymes. *Nat. Rev. Phys.* **2021,** *3* (4), 264-282 DOI: 10.1038/s42254-021-00289-3.

17.   Wernet, P. Chemical interactions and dynamics with femtosecond X-ray spectroscopy and the role of X-ray free-electron lasers. *Philos Trans A Math Phys Eng Sci* **2019,** *377* (2145), 20170464.

18.   Kraus, P. M.; Zurch, M.; Cushing, S. K.; Neumark, D. M.; Leone, S. R. The ultrafast X-ray spectroscopic revolution in chemical dynamics. *Nat. Rev. Chem.* **2018,** *2* (6), 82-94 DOI: 10.1038/s41570-018-0008-8.

19.   Chergui, M.; Collet, E. Photoinduced structural dynamics of molecular systems mapped by time-resolved X-ray methods. *Chem. Rev. (Washington, DC, U. S.)* **2017,** *117* (16), 11025-11065 DOI: 10.1021/acs.chemrev.6b00831.

20.   Chen, L. X. Ultrafast photochemical reaction trajectories revealed by X-ray transient absorption spectroscopy using X-ray free electron laser sources. *RSC Energy Environ. Ser.* **2017,** *18* (X-Ray Free Electron Lasers), 201-224.

21.   Seddon, E. A.; Clarke, J. A.; Dunning, D. J.; Masciovecchio, C.; Milne, C. J.; Parmigiani, F.; Rugg, D.; Spence, J. C. H.; Thompson, N. R.; Ueda, K.; Vinko, S. M.; Wark, J. S.; Wurth, W. Short-wavelength free-electron laser sources and science: a review. *Reports on Progress in Physics* **2017,** *80* (11), 115901 DOI: 10.1088/1361-6633/aa7cca.

22.   Huang, Z.; Kim, K.-J. Review of x-ray free-electron laser theory. *Physical Review Special Topics - Accelerators and Beams* **2007,** *10* (3), 034801 DOI: 10.1103/PhysRevSTAB.10.034801.

23.   Zhang, W.; Alonso-Mori, R.; Bergmann, U.; Bressler, C.; Chollet, M.; Galler, A.; Gawelda, W.; Hadt, R. G.; Hartsock, R. W.; Kroll, T.; Kjær, K. S.; Kubiček, K.; Lemke, H. T.; Liang, H. W.; Meyer, D. A.; Nielsen, M. M.; Purser, C.; Robinson, J. S.; Solomon, E. I.; Sun, Z.; Sokaras, D.; van Driel, T. B.; Vankó, G.; Weng, T.-C.; Zhu, D.; Gaffney, K. J. Tracking excited-state charge and spin dynamics in iron coordination complexes. *Nature* **2014,** *509* (7500), 345-348 DOI: 10.1038/nature13252.

24.   Wernet, P.; Kunnus, K.; Josefsson, I.; Rajkovic, I.; Quevedo, W.; Beye, M.; Schreck, S.; Grübel, S.; Scholz, M.; Nordlund, D.; Zhang, W.; Hartsock, R. W.; Schlotter, W. F.; Turner, J. J.;

Kennedy, B.; Hennies, F.; de Groot, F. M. F.; Gaffney, K. J.; Techert, S.; Odelius, M.; Föhlisch, A. Orbital-specific mapping of the ligand exchange dynamics of Fe(CO) 5 in solution. *Nature* **2015,** *520* (7545), 78-81 DOI: 10.1038/nature14296.

25.   Vankó, G.; Bordage, A.; Pápai, M.; Haldrup, K.; Glatzel, P.; March, A. M.; Doumy, G.; Britz, A.; Galler, A.; Assefa, T.; Cabaret, D.; Juhin, A.; van Driel, T. B.; Kjær, K. S.; Dohn, A.; Møller, K. B.; Lemke, H. T.; Gallo, E.; Rovezzi, M.; Németh, Z.; Rozsályi, E.; Rozgonyi, T.; Uhlig, J.; Sundström, V.; Nielsen, M. M.; Young, L.; Southworth, S. H.; Bressler, C.; Gawelda, W. Detailed Characterization of a Nanosecond-Lived Excited State: X-ray and Theoretical Investigation of the Quintet State in Photoexcited [Fe(terpy)2]2+. *The Journal of Physical Chemistry C* **2015,** *119* (11), 5888-5902 DOI: 10.1021/acs.jpcc.5b00557.

26.   Shelby, M. L.; Lestrange, P. J.; Jackson, N. E.; Haldrup, K.; Mara, M. W.; Stickrath, A. B.; Zhu, D.; Lemke, H. T.; Chollet, M.; Hoffman, B. M.; Li, X.; Chen, L. X. Ultrafast Excited State Relaxation of a Metalloporphyrin Revealed by Femtosecond X-ray Absorption Spectroscopy. *Journal of the American Chemical Society* **2016,** *138* (28), 8752-8764 DOI: 10.1021/jacs.6b02176.

27.   Ogi, Y.; Obara, Y.; Katayama, T.; Suzuki, Y.-I.; Liu, S. Y.; Bartlett, N. C.-M.; Kurahashi, N.; Karashima, S.; Togashi, T.; Inubushi, Y.; Ogawa, K.; Owada, S.; Rubešová, M.; Yabashi, M.; Misawa, K.; Slavíček, P.; Suzuki, T. Ultraviolet photochemical reaction of [Fe(III)(C2O4)3]3− in aqueous solutions studied by femtosecond time-resolved X-ray absorption spectroscopy using an X-ray free electron laser. *Structural Dynamics* **2015,** *2* (3), 034901 DOI: 10.1063/1.4918803.

28.   Miller, N. A.; Deb, A.; Alonso-Mori, R.; Garabato, B. D.; Glownia, J. M.; Kiefer, L. M.; Koralek, J.; Sikorski, M.; Spears, K. G.; Wiley, T. E.; Zhu, D.; Kozlowski, P. M.; Kubarych, K. J.; Penner-Hahn, J. E.; Sension, R. J. Polarized XANES Monitors Femtosecond Structural

Evolution of Photoexcited Vitamin B12. *Journal of the American Chemical Society* **2017,** *139* (5), 1894-1899 DOI: 10.1021/jacs.6b11295.

29.   Lemke, H. T.; Bressler, C.; Chen, L. X.; Fritz, D. M.; Gaffney, K. J.; Galler, A.; Gawelda, W.; Haldrup, K.; Hartsock, R. W.; Ihee, H.; Kim, J.; Kim, K. H.; Lee, J. H.; Nielsen, M. M.; Stickrath, A. B.; Zhang, W.; Zhu, D.; Cammarata, M. Femtosecond X-ray Absorption Spectroscopy at a Hard X-ray Free Electron Laser: Application to Spin Crossover Dynamics. *The Journal of Physical Chemistry A* **2013,** *117* (4), 735-740 DOI: 10.1021/jp312559h.

30.   Kunnus, K.; Vacher, M.; Harlang, T. C. B.; Kjær, K. S.; Haldrup, K.; Biasin, E.; van Driel, T. B.; Pápai, M.; Chabera, P.; Liu, Y.; Tatsuno, H.; Timm, C.; Källman, E.; Delcey, M.; Hartsock, R. W.; Reinhard, M. E.; Koroidov, S.; Laursen, M. G.; Hansen, F. B.; Vester, P.; Christensen, M.; Sandberg, L.; Németh, Z.; Szemes, D. S.; Bajnóczi, É.; Alonso-Mori, R.; Glownia, J. M.; Nelson, S.; Sikorski, M.; Sokaras, D.; Lemke, H. T.; Canton, S. E.; Møller, K. B.; Nielsen, M. M.; Vankó, G.; Wärnmark, K.; Sundström, V.; Persson, P.; Lundberg, M.; Uhlig, J.; Gaffney, K. J. Vibrational wavepacket dynamics in Fe carbene photosensitizer determined with femtosecond X-ray emission and scattering. *Nature Communications* **2020,** *11* (1), 634 DOI: 10.1038/s41467-020-14468-w.

31.   Kunnus, K.; Josefsson, I.; Rajkovic, I.; Schreck, S.; Quevedo, W.; Beye, M.; Weniger, C.; Grübel, S.; Scholz, M.; Nordlund, D.; Zhang, W.; Hartsock, R. W.; Gaffney, K. J.; Schlotter, W. F.; Turner, J. J.; Kennedy, B.; Hennies, F.; de Groot, F. M. F.; Techert, S.; Odelius, M.; Wernet, P.; Föhlisch, A. Identification of the dominant photochemical pathways and mechanistic insights to the ultrafast ligand exchange of Fe(CO)5 to Fe(CO)4EtOH. *Structural Dynamics* **2016,** *3* (4), 043204 DOI: 10.1063/1.4941602.

32.   Haldrup, K.; Gawelda, W.; Abela, R.; Alonso-Mori, R.; Bergmann, U.; Bordage, A.; Cammarata, M.; Canton, S. E.; Dohn, A. O.; van Driel, T. B.; Fritz, D. M.; Galler, A.; Glatzel, P.;

Harlang, T.; Kjær, K. S.; Lemke, H. T.; Møller, K. B.; Németh, Z.; Pápai, M.; Sas, N.; Uhlig, J.; Zhu, D.; Vankó, G.; Sundström, V.; Nielsen, M. M.; Bressler, C. Observing Solvation Dynamics with Simultaneous Femtosecond X-ray Emission Spectroscopy and X-ray Scattering. *The Journal of Physical Chemistry B* **2016,** *120* (6), 1158-1168 DOI: 10.1021/acs.jpcb.5b12471.

33.   Canton, S. E.; Kjær, K. S.; Vankó, G.; van Driel, T. B.; Adachi, S.-i.; Bordage, A.; Bressler, C.; Chabera, P.; Christensen, M.; Dohn, A. O.; Galler, A.; Gawelda, W.; Gosztola, D.; Haldrup, K.; Harlang, T.; Liu, Y.; Møller, K. B.; Németh, Z.; Nozawa, S.; Pápai, M.; Sato, T.; Sato, T.; Suarez-Alcantara, K.; Togashi, T.; Tono, K.; Uhlig, J.; Vithanage, D. A.; Wärnmark, K.; Yabashi, M.; Zhang, J.; Sundström, V.; Nielsen, M. M. Visualizing the non-equilibrium dynamics of photoinduced intramolecular electron transfer with femtosecond X-ray pulses. *Nature Communications* **2015,** *6* (1), 6359 DOI: 10.1038/ncomms7359.

34.   Biasin, E.; Fox, Z. W.; Andersen, A.; Ledbetter, K.; Kjær, K. S.; Alonso-Mori, R.; Carlstad, J. M.; Chollet, M.; Gaynor, J. D.; Glownia, J. M.; Hong, K.; Kroll, T.; Lee, J. H.; Liekhus-Schmaltz, C.; Reinhard, M.; Sokaras, D.; Zhang, Y.; Doumy, G.; March, A. M.; Southworth, S. H.; Mukamel, S.; Gaffney, K. J.; Schoenlein, R. W.; Govind, N.; Cordones, A. A.; Khalil, M. Direct observation of coherent femtosecond solvent reorganization coupled to intramolecular electron transfer. *Nature Chemistry* **2021,** *13* (4), 343-349 DOI: 10.1038/s41557-020-00629-3.

35.   Bokarev, S. I.; Kühn, O. Theoretical X-ray spectroscopy of transition metal compounds. *WIREs Computational Molecular Science* **2020,** *10* (1), e1433 DOI: https://doi.org/10.1002/wcms.1433.

36.   Ross, M.; Andersen, A.; Fox, Z. W.; Zhang, Y.; Hong, K.; Lee, J.-H.; Cordones, A.; March, A. M.; Doumy, G.; Southworth, S. H.; Marcus, M. A.; Schoenlein, R. W.; Mukamel, S.; Govind, N.; Khalil, M. Comprehensive Experimental and Computational Spectroscopic Study of

Hexacyanoferrate Complexes in Water: From Infrared to X-ray Wavelengths. *The Journal of Physical Chemistry B* **2018,** *122* (19), 5075-5086 DOI: 10.1021/acs.jpcb.7b12532.

37.   Van Kuiken, B. E.; Valiev, M.; Daifuku, S. L.; Bannan, C.; Strader, M. L.; Cho, H.; Huse, N.; Schoenlein, R. W.; Govind, N.; Khalil, M. Simulating Ru L3-Edge X-ray Absorption Spectroscopy with Time-Dependent Density Functional Theory: Model Complexes and Electron Localization in Mixed-Valence Metal Dimers. *The Journal of Physical Chemistry A* **2013,** *117* (21), 4444-4454 DOI: 10.1021/jp401020j.

38.   Tanaka, S.; Okada, K.; Kotani, A. Resonant X-Ray Emission Spectroscopy   in Dy Compounds. *Journal of the Physical Society of Japan* **1994,** *63* (7), 2780-2787   DOI: 10.1143/JPSJ.63.2780.

39.   Müller, P.; Neuba, A.; Flörke, U.; Henkel, G.; Kühne, T. D.; Bauer, M. Experimental and Theoretical High Energy Resolution Hard X-ray Absorption and Emission Spectroscopy on Biomimetic Cu2S2 Complexes. *The Journal of Physical Chemistry A* **2019,** *123* (16), 3575-3581 DOI: 10.1021/acs.jpca.9b00463.

40.   Heijboer, W. M.; Glatzel, P.; Sawant, K. R.; Lobo, R. F.; Bergmann, U.; Barrea, R. A.; Koningsberger, D. C.; Weckhuysen, B. M.; de Groot, F. M. F. Kβ-Detected XANES of Framework-Substituted FeZSM-5 Zeolites. *The Journal of Physical Chemistry B* **2004,** *108* (28), 10002-10011 DOI: 10.1021/jp048368w.

41.   Hämäläinen, K.; Siddons, D. P.; Hastings, J. B.; Berman, L. E. Elimination of the inner-shell lifetime broadening in x-ray-absorption spectroscopy. *Physical Review Letters* **1991,** *67* (20), 2850-2853 DOI: 10.1103/PhysRevLett.67.2850.

42.   Guo, M.; Prakash, O.; Fan, H.; Groot, L. H. M. d.; Freyr Hlynsson, V.; Kaufhold, S.; Gordivska, O.; Velásquez, N.; Chabera, P.; Glatzel, P.; Wärnmark, K.; Persson, P.; Uhlig, J.

HERFD-XANES probes of electronic structures of iron II/III carbene complexes. *Physical Chemistry Chemical Physics* **2020,** *22* (16), 9067-9073 DOI: 10.1039/C9CP06309A.

43. Bauer, M. HERFD-XAS and valence-to-core-XES: new tools to push the limits in research with hard X-rays? *Physical Chemistry Chemical Physics* **2014,** *16* (27), 13827-13837 DOI: 10.1039/C4CP00904E.

44. A. Lima, F.; Bjornsson, R.; Weyhermüller, T.; Chandrasekaran, P.; Glatzel, P.; Neese, F.; DeBeer, S. High-resolution molybdenum K-edge X-ray absorption spectroscopy analyzed with time-dependent density functional theory. *Physical Chemistry Chemical Physics* **2013,** *15* (48), 20911-20920 DOI: 10.1039/C3CP53133C.

45. Watzky, M. A.; Endicott, J. F.; Song, X.; Lei, Y.; Macatangay, A. Red-Shifted Cyanide Stretching Frequencies in Cyanide-Bridged Transition Metal Donor−Acceptor Complexes. Support for Vibronic Coupling. *Inorganic Chemistry* **1996,** *35* (12), 3463-3473 DOI: 10.1021/ic950834w.

46. Kaupp, M.; Renz, M.; Parthey, M.; Stolte, M.; Würthner, F.; Lambert, C. Computational and spectroscopic studies of organic mixed-valence compounds: where is the charge? *Physical Chemistry Chemical Physics* **2011,** *13* (38), 16973 DOI: 10.1039/c1cp21772k.

47. Glownia, J. M.; Gumerlock, K.; Lemke, H. T.; Sato, T.; Zhu, D.; Chollet, M. Pump–probe experimental methodology at the Linac Coherent Light Source. *Journal of Synchrotron Radiation* **2019,** *26* (3), 685-691 DOI: 10.1107/S160057751900225X.

48. Penfold, T. J.; Reinhard, M.; Rittmann-Frank, M. H.; Tavernelli, I.; Rothlisberger, U.; Milne, C. J.; Glatzel, P.; Chergui, M. X-ray Spectroscopic Study of Solvent Effects on the Ferrous and Ferric Hexacyanide Anions. *The Journal of Physical Chemistry A* **2014,** *118* (40), 9411-9418 DOI: 10.1021/jp5055588.

49. Aprà, E.; Bylaska, E. J.; Jong, W. A. d.; Govind, N.; Kowalski, K.; Straatsma, T. P.; Valiev, M.; Dam, H. J. J. v.; Alexeev, Y.; Anchell, J.; Anisimov, V.; Aquino, F. W.; Atta-Fynn, R.; Autschbach, J.; Bauman, N. P.; Becca, J. C.; Bernholdt, D. E.; Bhaskaran-Nair, K.; Bogatko, S.; Borowski, P.; Boschen, J.; Brabec, J.; Bruner, A.; Cauët, E.; Chen, Y.; Chuev, G. N.; Cramer, C. J.; Daily, J.; Deegan, M. J. O.; DunningJr., T. H.; Dupuis, M.; Dyall, K. G.; Fann, G. I.; Fischer, S. A.; Fonari, A.; Früchtl, H.; Gagliardi, L.; Garza, J.; Gawande, N.; Ghosh, S.; Glaesemann, K.; Götz, A. W.; Hammond, J.; Helms, V.; Hermes, E. D.; Hirao, K.; Hirata, S.; Jacquelin, M.; Jensen, L.; Johnson, B. G.; Jónsson, H.; Kendall, R. A.; Klemm, M.; Kobayashi, R.; Konkov, V.; Krishnamoorthy, S.; Krishnan, M.; Lin, Z.; Lins, R. D.; Littlefield, R. J.; Logsdail, A. J.; Lopata, K.; Ma, W.; Marenich, A. V.; Campo, J. M. d.; Mejia-Rodriguez, D.; Moore, J. E.; Mullin, J. M.; Nakajima, T.; Nascimento, D. R.; Nichols, J. A.; Nichols, P. J.; Nieplocha, J.; Otero-de-la-Roza, A.; Palmer, B.; Panyala, A.; Pirojsirikul, T.; Peng, B.; Peverati, R.; Pittner, J.; Pollack, L.; Richard, R. M.; Sadayappan, P.; Schatz, G. C.; Shelton, W. A.; Silverstein, D. W.; Smith, D. M. A.; Soares, T. A.; Song, D.; Swart, M.; Taylor, H. L.; Thomas, G. S.; Tipparaju, V.; Truhlar, D. G.; Tsemekhman, K.; Voorhis, T. V.; Vázquez-Mayagoitia, Á.; Verma, P.; Villa, O.; Vishnu, A.; Vogiatzis, K. D.; Wang, D.; Weare, J. H.; Williamson, M. J.; Windus, T. L.; Woliński, K.; Wong, A. T.; Wu, Q.; Yang, C.; Yu, Q.; Zacharias, M.; Zhang, Z.; Zhao, Y.; Harrison, R. J. NWChem: Past, present, and future. *The Journal of Chemical Physics* **2020,** *152* (18), 184102 DOI: 10.1063/5.0004997.

50. Valiev, M.; Bylaska, E. J.; Govind, N.; Kowalski, K.; Straatsma, T. P.; Van Dam, H. J. J.; Wang, D.; Nieplocha, J.; Apra, E.; Windus, T. L.; de Jong, W. NWChem: A comprehensive and scalable open-source solution for large scale molecular simulations. *Computer Physics Communications* **2010,** *181* (9), 1477-1489 DOI: DOI 10.1016/j.cpc.2010.04.018.

51.	Chollet, M.; Alonso-Mori, R.; Cammarata, M.; Damiani, D.; Defever, J.; Delor, J. T.; Feng, Y.; Glownia, J. M.; Langton, J. B.; Nelson, S.; Ramsey, K.; Robert, A.; Sikorski, M.; Song, S.; Stefanescu, D.; Srinivasan, V.; Zhu, D.; Lemke, H. T.; Fritz, D. M. The X-ray Pump–Probe instrument at the Linac Coherent Light Source. *Journal of Synchrotron Radiation* **2015,** *22* (Pt 3), 503-507 DOI: 10.1107/S1600577515005135.